LASER
& PHOTONICS
REVIEWS

Laser Photonics Rev. **10,** No. 6, 1600106 (2016) / **DOI** 10.1002/lpor.201600106

ORIGINAL
PAPER

Abstract We propose all-dielectric metasurfaces that can be actively re-configured using the phase-change material $Ge_2Sb_2Te_5$ (GST) alloy. With selectively controlled phase transitions on the composing GST elements, metasurfaces can be tailored to exhibit varied functionalities. Using phase-change GST rod as the basic building block, we have modelled meta-molecules with tunable optical response when phase change occurs on select constituent GST rods. Tunable gradient metasurfaces can be realized with variable supercell period consisting of different patterns of the GST rods in their amorphous and crystalline states. Simulation results indicate a range of functions can be delivered, including multilevel signal modulating, near-field coupling of GST rods, and anomalous reflection angle controlling. This work opens up a new space in exploring active meta-devices with broader applications that cannot be achieved in their passive counterparts with permanent properties once fabricated.

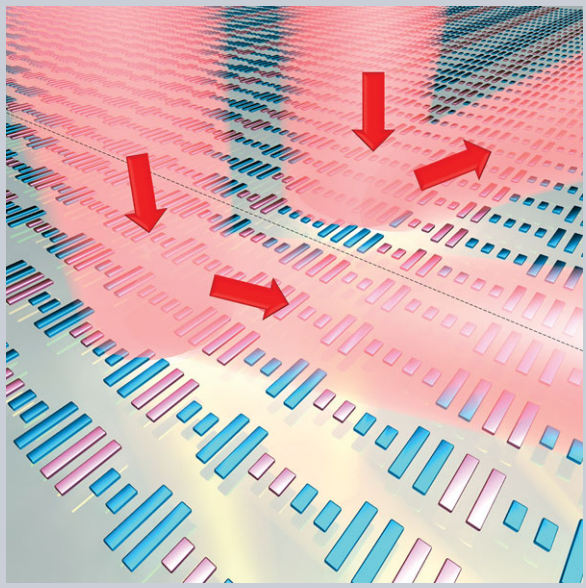

Active dielectric metasurface based on phase-change medium

Cheng Hung Chu[1], Ming Lun Tseng[2], Jie Chen[2], Pin Chieh Wu[1,2], Yi-Hao Chen[2], Hsiang-Chu Wang[1,2], Ting-Yu Chen[2], Wen Ting Hsieh[2], Hui Jun Wu[2], Greg Sun[3], and Din Ping Tsai[1,2,*]

1. Introduction

The development of flat and compact optical devices has drawn much interest owing to its potential applications in electromagnetic wave modulation. Much attention has been directed toward devices made of either metamaterials or metasurfaces consisting of ultrathin artificial subwavelength structures. Metamaterials have been shown to demonstrate many exotic optical properties, such as electromagnetically induced transparency (EIT) [1–4], optical Fano resonance [5–8], optical super absorber [9, 10], giant nonlinearity [11, 12], and optical negative refraction [13–15] among others [16]. However, because of the tremendous loss associated with the metal components embedded in these three-dimensional (3D) structures, metamaterials have little chance to be employed in applications where efficiency is a matter of concern. To this end, metasurfaces [17–19], the two-dimensional (2D) version of the metamaterial, where light is not required to have a deep penetration, have been used to show exceptional functionalities in manipulating various optical properties, such as flat lens [20, 21], meta-hologram [22, 23], and polarization control [18, 24]. While metasurfaces have demonstrated better performance in efficiency by comparison with the 3D metamaterials, the loss is still a significant concern because of the metal elements commonly used here [25, 26]. It is therefore desirable to do away with any metal altogether by applying the all-dielectric approach [27–30]. For example, using stacked silicon rods, zero-index low-loss metamaterial at optical frequency has been realized, and the modulation of the light emission from the quantum dots nearby this metamaterial has been demonstrated [30]. Also, low-loss EIT metasurface consisting of silicon nanoantenna for refractive index sensing is demonstrated recently [29]. The other limitation with the conventional metasurfaces is that their optical properties are typically permanent once the devices are fabricated. There is obviously a need to develop tunable all-dielectric "meta-devices" [31–33] where their

[1] Research Center for Applied Sciences, Academia Sinica, Taipei 115, Taiwan
[2] Department of Physics, National Taiwan University, Taipei 106, Taiwan
[3] Department of Engineering, University of Massachusetts Boston, MA, 02125, U.S.A
*Corresponding author: dptsai@phys.ntu.edu.tw

This is an open access article under the terms of the Creative Commons Attribution-NonCommercial-NoDerivs License, which permits use and distribution in any medium, provided the original work is properly cited, the use is non-commercial and no modifications or adaptations are made.

© 2016 The Authors. Laser & Photonics Reviews published by Wiley-VCH Verlag GmbH & Co. KGaA Weinheim.

optical responses can be actively controlled with external applied measures, such as force, heat, electric or magnetic field. One kind of material that can be conveniently applied to achieve such a unique feature is the phase-change media which exhibit dramatic difference in optical and electrical characteristics between its crystalline and amorphous states [34]. The phase transition can be induced by applying either heat [35], photon [36, 37], or electric energy [38–40] on the phase-change material. The reversibility between phase states can be realized by carefully modulating input energy pulse [41, 42]. Such phase-change materials have been widely used in commercial rewritable optical disks [36] and as media for storage cells in electronic phase-change memories [39, 40]. These properties can provide active modulation or switching when applied properly to metasurfaces. So far, most studies concerning phase-change materials only employ them as surrounding medium for metallic subwavelength structures by using their dielectric constant change to tune the plasmonic resonance for optical switching [43–46]. For example, by placing metasurface on the phase-change medium, the Fano resonances on the metasurfaces can be tuned reversibly, resulting in a high-contrast optical signal modulation [43, 45]. These metamaterials still use metal to generate plasmonic resonances with phase-change medium acting as background, as a result, they are lossy. An interesting question naturally arises – whether phase change materials can be used in place of metal on metasurfaces. Among the many different phase-change materials, $Ge_2Sb_2Te_5$ (GST) alloy is known to have advantages of low optical loss in the near infrared (NIR) range and non-volatility, high stability and quick response [43, 47]. To this end, artificially structured GST presents an interesting opportunity. In this paper, we study the fundamental optical response of the GST system made into unit blocks from which metasurfaces are constructed with properties that are not only otherwise nonexistent in nature but also controllable, with the goal to demonstrate reconfigurable meta-devices in NIR utilizing its tunable optical properties as it undergoes phase transition. We first numerically analyze the optical resonant modes associated with the GST rod as an optical dipole antenna with different crystallization levels. Based on this, we then propose a metasurface composed of addressable meta-molecules with constituent GST rods. Near-field coupling between the GST rods within a meta-molecule can be tuned by modifying the phase state of these GST rods. Finally, we validate the concept of reconfigurable gradient metasurface capable of exhibiting different anomalous reflection angles by controlling the combination of GST rods with different geometries and phase states. Such an active metasurface opens up the potential for tunable meta-devices with broader applications that cannot be realized in their passive counterparts with permanent properties once they are made.

2. Optical properties of GST rod

Experimental and theoretical investigations of the optical constants/dielectric functions of GST have been previously

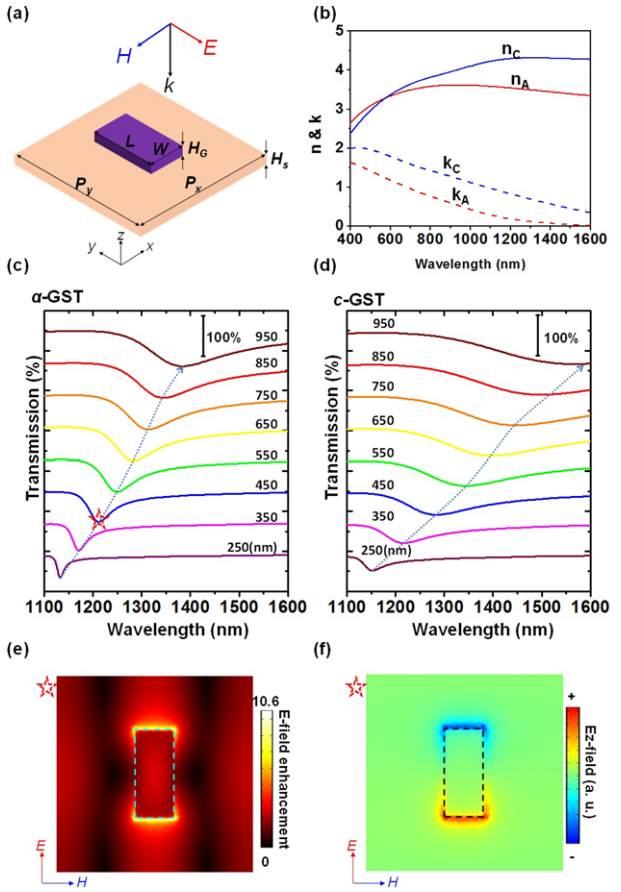

Figure 1 Phase-change rod. (a) Schematic of the GST rod on freestanding SiN_x thin film (unit cell) $P_x = P_y = 1000$nm, $W = 250$nm, $H_G = 50$nm, $H_S = 50$nm. The rod length L is varied from 250 nm to 950 nm. (b) Optical constants of GST in amorphous and crystalline states. n_A and k_A are the refractive index and extinction coefficient of α-GST, n_C and k_C are those of c-GST, respectively [43]. Transmission spectra of the α-GST (c) and c-GST rod arrays (d) of different length L. (e) Electric field enhancement and (f) z-direction electric field distribution of the α-GST rod with $L = 450$ nm, where the three-dimensional axes are shown in (a).

reported [48, 49]. Figure 1a shows the schematic of a GST rod as a unit block which behaves as an antenna that couples with the incident electromagnetic wave. We use the ellipsometrically measured refractive indices as well as extinction coefficients of GST in amorphous state and crystalline state as shown in Fig. 1b [43]. The GST rod is sitting on a free-standing silicon nitride (SiN_x) substrate (thickness = 50 nm) which is commercially available. Free-standing SiN_x thin film is a good choice as substrates for ultrathin dielectric metasurface devices. In fact, SiN_x thin film has been widely used in the development of thin metamaterial and metasurface devices [31, 50] because of its small surface roughness and near zero extinction in visible and near-IR regime. Electromagnetic simulation softwares Comsol (based on the finite element method) and CST (based on finite-difference time-domain method) are employed for the calculation of optical properties of the GST structure. The

© 2016 The Authors. Laser & Photonics Reviews published by Wiley-VCH Verlag GmbH & Co. KGaA Weinheim.

optical transmission spectra of a α-GST rod with various lengths L are shown in Figure 1c. When the incident polarization is parallel to the long axis of the rod, an obvious resonant feature can be found in each spectrum. The resonant wavelength of the rod is red-shifted with the increase of L. This relation is in good agreement with the theoretical prediction on the resonant properties of dielectric resonator, which can be described by: $p(\lambda/n) \approx 2\pi L$, where p is a positive integer, and n is the refractive index of GST at the resonance wavelength [51,52]. We have analyzed the near-field distributions of different resonant modes arisen from the oscillation of the induced displacement currents in the GST rod. Figures 1e and 1f are the simulation results for the case of α-GST antenna with $L = 450$ nm. The field distribution in Figure 1e shows the typical characteristics of electric dipolar resonance of the GST rod at the resonant wavelength $\lambda = 1235$ nm, where the field is strongly localized near the short edges (top and bottom ends). The enhancement of electric field can be as high as $\sim$ 10-fold relative to the incident field. In contrast, the resonant dip of c-GST rod is red-shifted in comparison with that of α-GST rod of equal length. This result is associated to the increment of refractive index n of GST after phase transition from amorphous to crystalline state which is similar to what has been shown by Mie scattering theory that the optical resonance of a dielectric nanosphere also red-shifts with the increasing refractive index n of the material.

The optical/electrical multi-level states is an important characteristic of GST [54]. By controlling the applied energy on the GST rod, partial crystalline state due to the formation of nucleation in amorphous GST can be realized [53,54]. The optical resonances of phase-change metasurfaces can thus be gradually tuned by employing this method. Among the several effective-medium theories developed for the description of the optical constants/dielectric functions of heterogeneous medium [55,56], Lorentz-Lorenz relation [57] is one of the best candidates that has been successfully applied in the simulation of the Au nanodisks/GST thin film hybrid system in which the GST thin film is in different crystallization ratio [44]. Figure 2 shows the transmission spectra of a phase-change GST rod (length: 850 nm) with a crystallization fraction of 0% (α-GST), 25%, 50%, 75%, and 100 % (c-GST). The effective dielectric constant of the GST material in different crystallization conditions can be approximated using the Lorentz-Lorenz relation,

$$\frac{\varepsilon_{eff}(\lambda)-1}{\varepsilon_{eff}(\lambda)+2} = m \times \frac{\varepsilon_{CGST}(\lambda)-1}{\varepsilon_{CGST}(\lambda)+2} + (1-m) \times \frac{\varepsilon_{AGST}(\lambda)-1}{\varepsilon_{AGST}(\lambda)-1}, \quad (1)$$

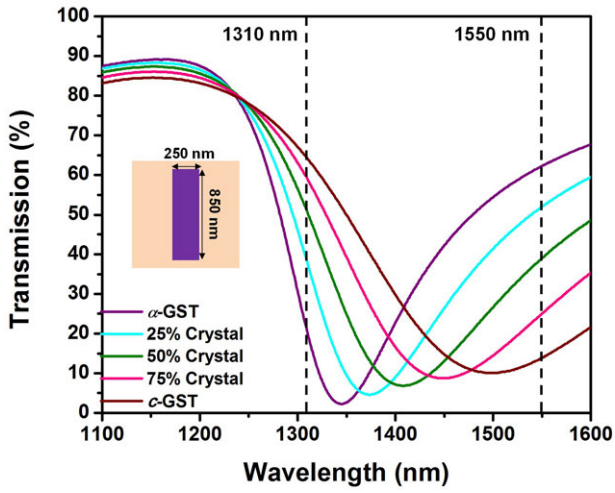

Figure 2 Tuning of the transmission spectrum of GST rod array with the control of its crystallization fraction. Transmission spectra of GST rod with different crystallization fraction. By changing the crystallization fraction of GST rod, the resonance wavelength can be gradually tuned. Five transmission levels can be clearly observed at 1310 nm and 1550 nm.

where $\varepsilon_{CGST}(\lambda)$ and $\varepsilon_{AGST}(\lambda)$ are the wavelength (λ)-dependent dielectric constants of GST in crystalline and amorphous state, respectively, and m is the crystallization fraction of the GST, ranging from 0 to 1. The electric dipole resonance of the GST rod is shifted toward longer wavelength with the increase of m. As can be seen in Figure S1 in supporting information, which is the change of the transmission versus wavelength under different crystallization ratio, by controlling crystallization ratio, multi-level optical signal modulation at a specific wavelength can be achieved. For example, five transmission levels can be clearly observed at $\lambda = 1310$ nm and $\lambda = 1550$ nm (see Table 1).

3. Tuning the EIT resonance on phase-change metamolecule by selective modification

Optical properties of metamolecules that are created artificially can be engineered through the design of geometrical parameters of their constituent "meta-atoms" inside [58–61]. Here we demonstrate through numerical simulation that properties of a metamolecule can be tailored actively by manipulating the phase states of its constituent GST rods that work as "meta-atoms".

Table 1 Transmission coefficients of GST rod array with different crystallization fraction at $\lambda = 1310$ nm and $\lambda = 1550$ nm

Phase state	α-GST	25% Crystal	50% Crystal	75% Crystal	c-GST
Transmission at 1310 nm (%)	20.15	37.71	50.51	58.9	64.15
Transmission at 1550 nm (%)	56.25	43.85	29.35	16.45	10.33

© 2016 The Authors. Laser & Photonics Reviews published by Wiley-VCH Verlag GmbH & Co. KGaA Weinheim.

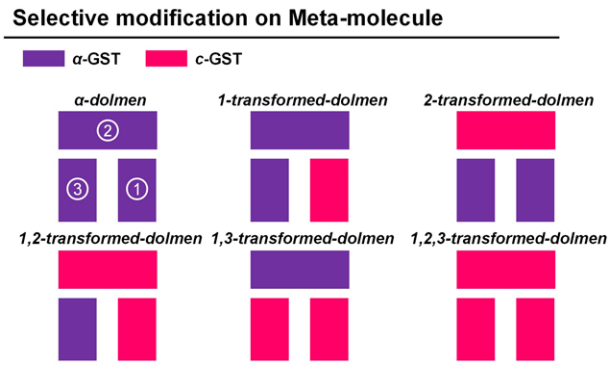

Figure 3 Designation of the dolmen metamolecule with different composition of rod phase states that mimics the denomination principle used in the organic chemistry.

Figure 3 shows the scheme of selective modification of a phase-change metasurface in which the well-known dolmen structure [4] is employed. The dolmen metamolecule is composed of a horizontal rod working as dipole antenna and a pair of vertical rods as quadrupole antenna. Following the denomination rules in organic chemistry, the metamolecule is labeled in terms of its phase states of composing GST rods. For example, when one of the vertical rods is modified from the amorphous state into crystalline state, the metamolecule is named as 1-transformed-dolmen. When one of the vertical rods and the horizontal rod are both in crystalline state, the metamolecule is labeled as 1,2-transformed-dolmen.

The geometrical parameters and optical transmission spectra of the α-dolmen metamolecule are shown in Figures 4a and 4b, respectively. The polarization of the normal incident light is along the long axis of the horizontal rod. Within the wavelength regime of 1400–1600 nm, an EIT-like spectral profile centered at around 1483 nm is identified (marked with a star). The electromagnetic field distribution of the dolmen metamolecule around the EIT-like peak is shown in Figures 4c and 4d. One can easily identify the electric quadrupole within the metamolecule through the near-field coupling between the GST rods [2,4]. Interestingly, the full-width-at-half-maximum (FWHM) of the EIT-like peak is around 50 nm. The FWHM of the EIT-like peak is much narrower than that of a similar dolmen metamolecule made of gold rods (FWHM: ~235 nm, see the discussion in the supporting information Figures S2-S3), which is a result of GST being a dielectric medium with far less loss than metal of any kind.

When the phase state in one of the GST rods inside the metamolecule is modified, the optical resonance of the metamolecule changes dramatically. The middle and bottom panels in Figure 4b show the transmission spectra of the 1-transformed-dolmen and 2-transformed-dolmen, respectively. The optical spectrum is significantly changed when the phase state of any rod in the metamolecule is modified. In the case of 1-transformed-dolmen, the transmission spectrum exhibits a similar EIT-like profile as that of α-dolmen, but the resonant features are red-shifted and relatively broader. In order to clarify the impact of phase state of each rod to the resonant modes, the optical responses of the α-GST and 1-transformed-GST rod pair are simulated and the results are shown in Figure S4. The incident light is illuminated on the metamolecule with a titled angle of 35° to excite the quadrupole mode in the metamolecule [4]. It can be seen in Figure S4b that the resonant dip associated with the quadrupole mode of the 1-transformed-GST rod pair is broader than that of the α-GST rod pair. This result can be attributed to the increased extinction coefficient of the GST rod that is in the crystalline state. Because the EIT-like spectral profile of dolmen metamolecule is the result of interference between the excitation pathways of dipole and quadrupole modes inside it [2], the modification of quadrupole resonance induces apparent variation in the spectral profile. Therefore, the resonant profile of 1-transformed-dolmen becomes broader than that of α-dolmen. In the case of 2-transformed-dolmen, the EIT-like resonance disappears, leaving only the dipole resonance

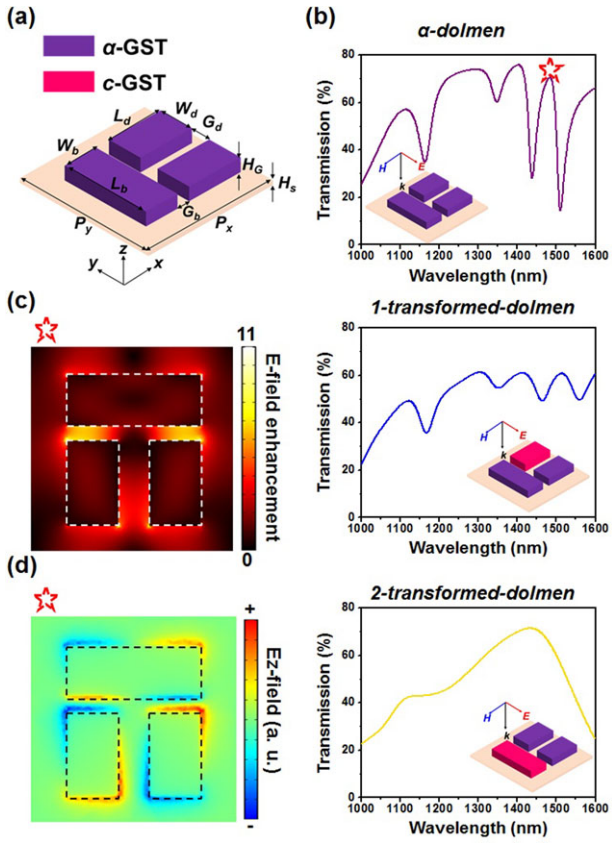

Figure 4 Active control of the Fano resonance by the phase-change dolmen metamolecule. (a) Geometrical parameters of the dolmen metamolecule. $P_x = P_y = 1000$ nm. $L_b = 650$ nm, $L_d = 420$nm, $W_b = W_d = 300$ nm, $G_b = 70$nm, $G_d = 150$nm, $H_G = 150$nm, $H_S = 50$nm. (b) Transmission spectra of α-dolmen, 1-transformed-dolmen, and 2-transformed-dolmen metamolecules with purple and pink indicating amorphous and crystalline state, respectively. (c) Electric field intensity and (d) z-component electric field strength around the α-dolmen metamolecule at its EIT-like resonance, where the z-axis is denoted in (a).

© 2016 The Authors. Laser & Photonics Reviews published by Wiley-VCH Verlag GmbH & Co. KGaA Weinheim.

Table 2 Transmission coefficients of dolmen meta-molecule arrays with different modification conditions at $\lambda = 1250$ nm

Phase state	Transmission (%)
α-dolmen	72.59
1-transformed dolmen	56.88
2-transformed dolmen	49.42
1,2-transformed dolmen	39.33
1,3-transformed dolmen	43.94
1,2,3-transformed dolmen	30.24

from the horizontal rod. Due to the large difference in the resonant wavelengths between the dipole and quadrupole modes, the energy transfer between them becomes much weaker, resulting in the disappearance of the EIT-like spectral profile [5], which can be understood in the comparison of the bottom panel of Figure S4b and the top panel of Figure S4c. The above analysis indicates that using selective modification of the phase state of the GST rods within the metamolecule, one can not only control its resonant wavelength but also resonance strength. Figure S5 shows the transmission spectra of GST dolmen metasurface under different modification conditions, where Table 2 shows the transmission at $\lambda = 1250$ nm of the dolmen metasurface under different phase-state modification conditions in which obvious transmission changes can be observed. It is not difficult to see from the result in Table 2, that we can use far-field spectroscopy technique to reveal information on phase compositions of the GST metasurface without employing more complex and costly near-field optical spectroscopy [62] or the electronic technique, such as conductive-AFM technique [38].

We now show another unique feature of the phase-change metasurface that cannot be observed in conventional metasurfaces made of metals. Considering the case of a metamolecule composed of two identical metal rods placed in parallel, due to the geometrical symmetry, the quadrupole mode cannot be excited with normal incident light polarized along the long axis of the rods [3]. To excite such a mode, one has to break the geometrical symmetry of the two rods within the metamolecule [3, 59]. With the use of the phase-change GST, such a symmetry can be easily broken with the change of phase state of one of the rods to allow for quadrupole mode be excited so that EIT-like resonance can be observed under the excitation condition that is impossible in metallic metamaterials. Figure S6a shows the schematic of the dolmen metamolecule with slightly modified geometry. The separation between the two vertical rods is decreased to 50 nm. The transmission spectra of the α-dolmen and 1-transformed-dolmen are shown in Figure S6a where the polarization of the normal incident light is perpendicular to the long axis of the horizontal rod. In the case of α-dolmen, only electric dipole resonance is observed, while in the 1-transformed-dolmen, the EIT-like resonance is clearly revealed because of the broken symmetry.

The electric field distribution at the transmission peak ($\lambda = 1430$nm) of the EIT-like resonance for the 1-transformed-dolmen in Figure S6c shows antisymmetric electric fields around the two vertical rods, indicating excitation of the quadrupole mode. The out-of-phase electric dipole oscillation in the rods is attributed to the asymmetry of the phase states in the vertical rods that results in phase difference between the resonances in the two rods under normal incident excitation. The EIT-like resonance observed is thus related to the interference between the "bonding" and "anti-bonding" modes [59, 63] associated with the two GST rods in different phase states.

4. Tuning the anomalous reflection on phase-change metasurface

In addition to the control of optical resonance, selective modification of the phase-states of GST rods can also be applied to the application of wave-front modulation by the metasurface composed of such phase-change GST rods. Figure 5 illustrates the construction and switching mechanism of the proposed phase-change gradient-index metasurface operating at 1550 nm. The phase-change rods are used as the basic building block for controlling the light phase and intensity of the so-called anomalous reflection induced by metasurface [64] by tuning their phase state and geometry to construct the needed gradient indices on

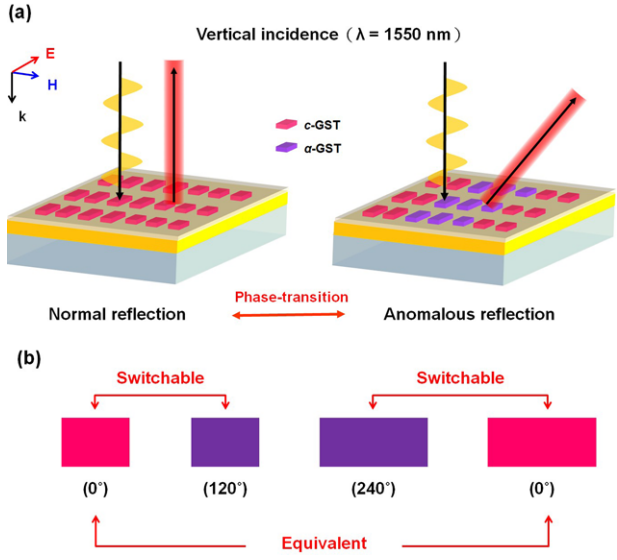

Figure 5 Tunable gradient metasurface. (a) Illustration of the tunable phase change gradient metasurface working principle. The reflective metasurface consists of an array of GST nanorods with different phase states and a continuous Au mirror separated by a spacer layer. Under the illumination of a normal incidence (1550 nm), the metasurface can switch its reflection angle by modulating the phase state of each GST nanorod. (b) Selection rule for the unit cell of gradient metasurface. By changing the phase states of two different geometries GST rods, a three-level gradient phase modulation can be realized.

© 2016 The Authors. Laser & Photonics Reviews published by Wiley-VCH Verlag GmbH & Co. KGaA Weinheim.

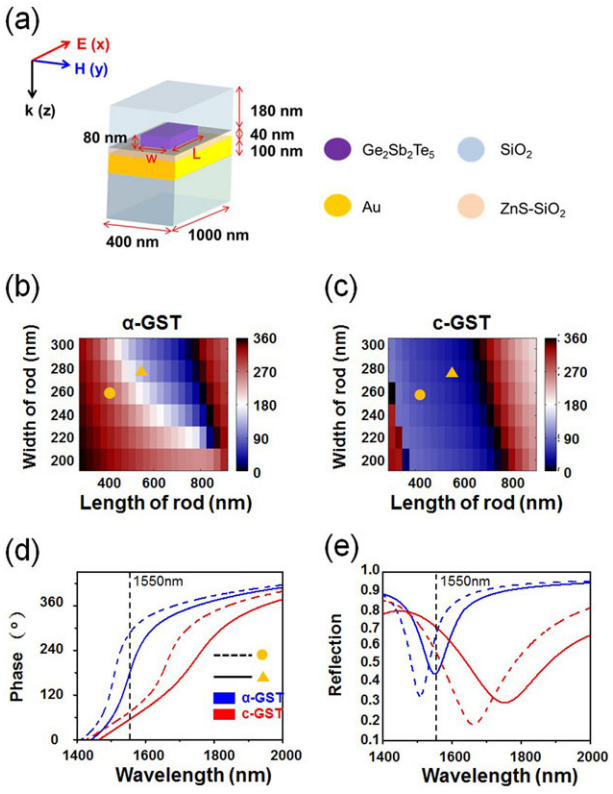

Figure 6 Design of tunable gradient metasurface. (a) Schematic diagram of a basic unit cell consisting of a GST nanorod (length L, width W, and height 80nm) on top of a 40 nm ZnS-SiO_2 spacer and gold substrate. (b-c) Phase of the reflected light as the function of width W and length L of amorphous and crystalline GST nanorod at a wavelength of 1550nm. (d-e) Reflection phase and relative intensity of two selected GST nanorods with width and length of (260nm, 420nm) & (280nm, 510nm).

the metasurface. The reflection can be directed to desired angles by changing the phase states of select rods shown in Figure 5a. Two amorphous rods with different geometries are chosen at a particular wavelength to yield an initial phase difference of 120˚. Meanwhile, the phase difference between their amorphous and crystalline state is also 120˚. The switching functionality achieved with the three-level phase modulation is shown in Figure 5b.

One building block as shown in Figure 6a occupying an area of 1000×400 nm^2 consists of a SiO_2 layer (180 nm), a GST rod (length: L nm, width: W nm), ZnS-SiO_2 spacer (40 nm), and Au mirror (100 nm) at the bottom. The Au thin film serves as a reflecting mirror to increase the interaction cross section between the GST rods and the incident wave [64]. The ZnS-SiO_2 spacer is important for controlling the coupling between the Au mirror and GST rods. All GST rods have a fixed thickness of 80 nm while L and W are varied to produce the desired phase modulation across the metasurface. The refractive indices of SiO_2 and ZnS-SiO_2 are 1.45 and 2 [65], respectively. Figures 6b and 6c are the optical phase responses of a metasurface consisting of either amorphous or crystalline GST rods, respectively, as a function of L and W at the incident wavelength of 1550 nm. The polarization of incident light is parallel to the long axis of GST rods. Each GST rod here works as a dipole antenna capable of modulating both the amplitude and phase of the reflected wave. Optical phase modulation as large as 2π by tuning L and W can be achieved. Figures 6d and 6e show the optical phase response and reflection of GST rods with the dimensions of $420\times260\times80$ nm^3 (dotted line) and $510\times280\times80$ nm^3 (solid line) in crystalline (red line) and amorphous states (blue line), respectively. The abrupt optical phase shifts occur at dipole resonances. When GST rods are all in crystalline state, resonances are far away from 1550 nm and the optical phase shift varies slowly with the wavelength. In contrast, the dipole resonances of α-GST rods are much closer to 1550 nm and their optical phase shifts are far more sensitive to wavelength change.

These GST rods in different phase states can be arranged to form the so-called supercells from which a tunable phase-change metasurface can be designed based on the generalized Snell's law [18],

$$\sin\theta_r - \sin\,\theta_i = \frac{\lambda}{2\pi}\,\frac{d\varphi}{dy}, \tag{2}$$

where the reflection angle θ_r and incident angle θ_i are related by the phase gradient dφ/dy along the y-direction. In the case of normal incidence ($\theta_i = 0^\circ$) and 2π optical phase change over the period of a supercell L_S, dφ/dy $= 2\pi/L_S$ [66], and the reflection angle can be simply determined by Ls,

$$\theta_r = \sin^{-1}\left(\frac{\lambda}{L_s}\right), \tag{3}$$

Figure 7 illustrates three designs of the tunable gradient metasurfaces, each with different supercell period. Figure 7a shows a supercell design with twelve c-GST rods of two different geometries, the period of such a supercell is much larger than the incident wavelength and can be considered as infinitely large in practical sense. Changing the phase state of 6 rods into amorphous state as shown in Figure 7b, we arrive at a metasurface with the supercell period of 2400 nm. In a different combination, eight amorphous and four c-GST rods produce a supercell with the period of 4800nm. Obviously, there are other configurations that can be obtained with the active control of the phase change on each GST rod, and the result is abundant collection of interesting optical responses yielded from a single tunable metasurface. For example, the anomalous reflection for a normal incident light at 1550 nm for the three cases described above is clearly directed onto different angles of 0˚, -40˚ and -20˚ as shown in Figure 8a. This numerical result is in excellent agreement with Equation (3). As expected, when the supercell period is large relative to the incident wavelength and can be approximated as infinite, the metasurface reflects the normal incident wave back at the same normal angle of 0°. This is also confirmed with the reflection wave-front being parallel to the metasurface plane as shown in Figure 8b. The wave-fronts for the other

© 2016 The Authors. Laser & Photonics Reviews published by Wiley-VCH Verlag GmbH & Co. KGaA Weinheim.

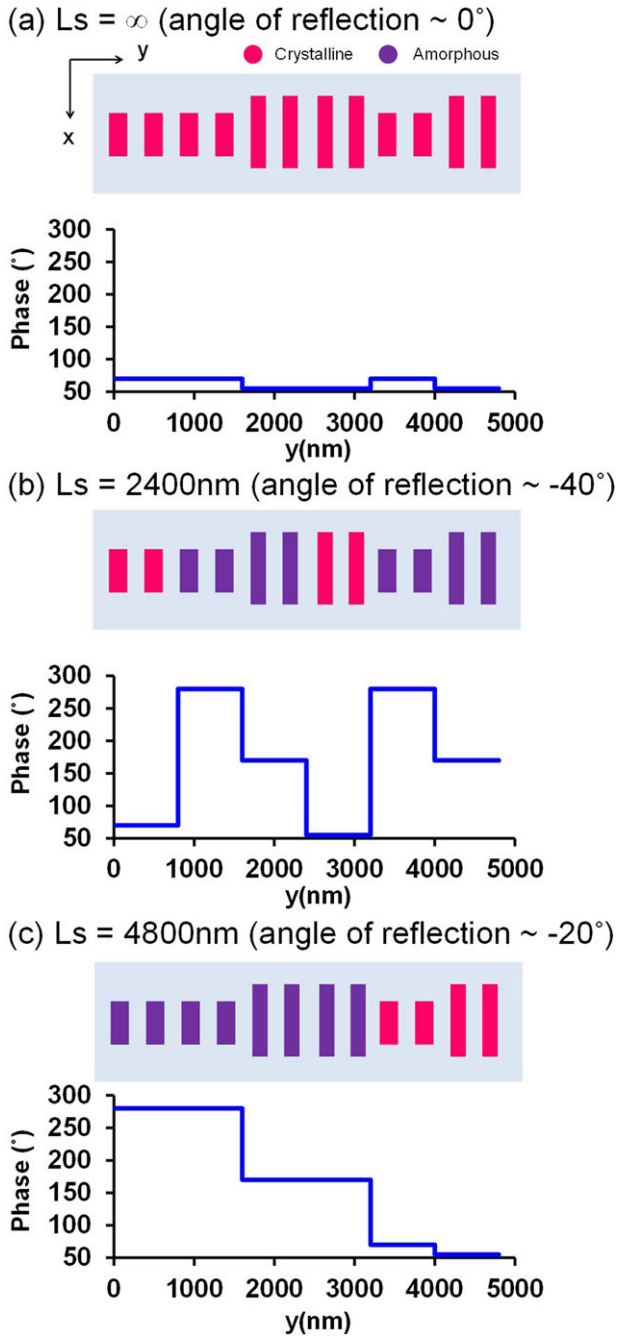

Figure 7 Supercell Design of tunable gradient metasurface. Patterns of GST nanorods are shown with the superlattice periodicity Ls of (a) ∞, (b) 2400 nm, (c)4800 nm, and their corresponding phase distribution represented as step function by the blue lines.

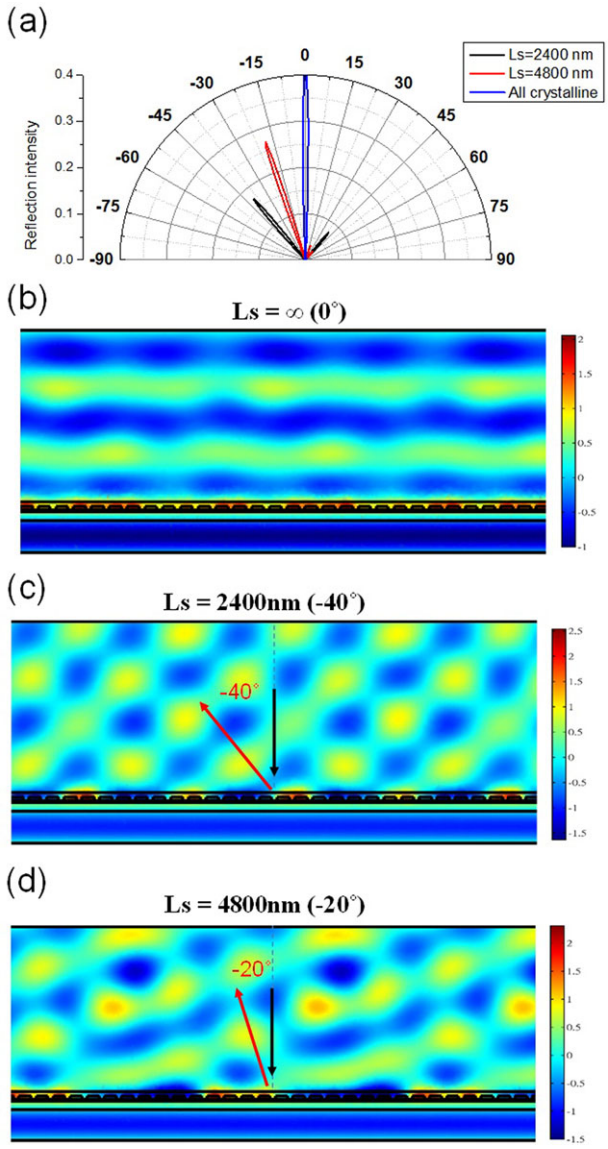

Figure 8 Tunability of the anomalous reflection of phase-change metasurface. (a) Scattered electric field intensity pattern and (b-d) the corresponding wave front of E_y component plotted in the x-z plane for the normal incident with Ls = ∞, 2400nm and 4800nm (λ=1550 nm).

two cases with the reflection angles of -40° and -20° are shown in Figures 8c and 8d. The simulation results are in good agreement with Equation (3). There are, however, some small unintended reflection peaks at 20° or 40° which we have not been able to completely suppress due to grating diffractions by the supercells.

To realize the selective modification technique on the proposed phase-change metasurface, several matured techniques used in phase-change-material-based technologies can be adopted. One of the possible methods based on phase-change electronic memory is plotted in Figure 9. The meta-atoms of the phase-change metasurface are made on the TiN electrodes (for converting the electronic energy to thermal energy) which are connected with the conducting wire. By applying electronic pulse on the specific meta-atoms, the phase state of the treated meta-atoms can be changed, resulting in the selective modification on the metasurface-based device. Other possible methods can be the conductive-AFM [38], laser-direct writing [67–69], and so on.

© 2016 The Authors. Laser & Photonics Reviews published by Wiley-VCH Verlag GmbH & Co. KGaA Weinheim.

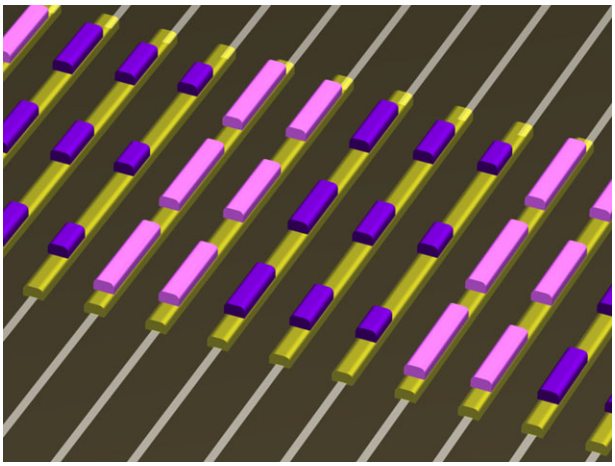

Figure 9 Schematics for realization of the selective modification of phase-change metasurface. The GST rods of the metasurface are deposited on TiN electrode (shown in gold color), and their phase states can be changed by applying electric current pulses through the conductive wire.

5. Conclusion and outlook

In conclusion, using numerical simulation we have demonstrated that the all-dielectric phase-change material GST can be used to obtain reconfigurable metasurfaces with functional diversity for light modulation. The switchable electric dipole resonance of phase-change rods are presented. In addition to phase transitions between amorphous and crystalline state, partial crystallization in GST can also be used to increase the tuning range and resolution of the metasurfaces for more complex light modulation. Using GST rod as the basic building block, we have designed a single metasurface that is capable of exhibiting tunable optical response when selected GST rods underwent phase change. Such a tunable, all-dielectric metasurface offers superior properties and performance over the conventional metal metasurfaces that are known to be inherently inefficient and untunable. This design work is intended to shed light on the use of phase-change GST for active metasurfaces and stimulate future experimental demonstration of such devices that go far beyond the conventional metasurfaces in terms of functionality.

Supporting Information

Additional supporting information may be found in the online version of this article at the publisher's website.

Acknowledgements. The authors acknowledge financial support from Ministry of Science and Technology, Taiwan (Grant No. MOST-105-2745-M-002-002-ASP and 105-2917-I-564-019-) and Academia Sinica (Grant No. AS-103-TP-A06). They are also grateful to National Center for Theoretical Sciences, Molecular Imaging Center of National Taiwan University, National Center for High-Performance Computing, Taiwan, and Research Center for Applied Sciences, Academia Sinica, Taiwan for their supports. G. Sun acknowledges support from AFOSR (FA9550-14-1-0196, Dr. Gernot Pomrenke, Program Manager) and AOARD (FA2386-16-1-4069 FA2386-14-1-4073, Dr. Kenneth Caster, Program Manager). M. L. Tseng thanks Profs. Peter Nordlander and Naomi Halas in Rice University for their helpful discussions. C. H. Chu, M. L. Tseng and J. Chen contributed equally to this work.

Received: 25 April 2016, **Revised:** 21 August 2016, **Accepted:** 22 September 2016

Published online: 13 October 2016

Key words: reconfigurable metasurface, metamaterials, beam steering, Fano resonances, phase-change material.

References

[1] N. J. Halas, S. Lal, W.-S. Chang, S. Link, and P. Nordlander, Chem. Rev. **111**, 3913–3961 (2011).
[2] N. Liu, L. Langguth, T. Weiss, J. Kastel, M. Fleischhauer, T. Pfau, and H. Giessen, Nat. Mater. **8**, 758–762 (2009).
[3] Z.-G. Dong, H. Liu, M.-X. Xu, T. Li, S.-M. Wang, S.-N. Zhu, and X. Zhang, Opt. Express **18**, 18229–18234 (2010).
[4] S. Zhang, D. A. Genov, Y. Wang, M. Liu, and X. Zhang, Phys. Rev. Lett. **101**, 047401 (2008).
[5] B. Luk'yanchuk, N. I. Zheludev, S. A. Maier, N. J. Halas, P. Nordlander, H. Giessen, and C. T. Chong, Nat. Mater. **9**, 707–715 (2010).
[6] M. Rahmani, B. Luk'yanchuk, and M. Hong, Laser Photonics Rev. **7**, 329–349 (2013).
[7] B. Hopkins, A. N. Poddubny, A. E. Miroshnichenko, and Y. S. Kivshar, Laser Photonics Rev. **10**, 137–146 (2016).
[8] X. Fang, M. L. Tseng, D. P. Tsai, and N. I. Zheludev, Phys. Rev. Applied **5**, 014010 (2016).
[9] Y. Cui, Y. He, Y. Jin, F. Ding, L. Yang, Y. Ye, S. Zhong, Y. Lin, and S. He, Laser Photonics Rev. **8**, 495–520 (2014).
[10] F. Ding, Y. Jin, B. Li, H. Cheng, L. Mo, and S. He, Laser Photonics Rev. **8**, 946–953 (2014).
[11] A. Ciattoni, C. Rizza, A. Marini, A. D. Falco, D. Faccio, and M. Scalora, Laser Photonics Rev. **10**, 517–525 (2016).
[12] M. Ren, E. Plum, J. Xu, and N. I. Zheludev, Nat. Commun. **3**, 833 (2012).
[13] V. M. Shalaev, Nat. Photonics **1**, 41–48 (2007).
[14] J. Valentine, S. Zhang, T. Zentgraf, E. Ulin-Avila, D. A. Genov, G. Bartal, and X. Zhang, Nature **455**, 376–379 (2008).
[15] V. Klimov, S. Sun, and G.-Y. Guo, Opt. Express **20**, 13071–13081 (2012).
[16] W. Liu, J. Zhang, and A. E. Miroshnichenko, Laser Photonics Rev. **9**, 564–570 (2015).
[17] A. V. Kildishev, A. Boltasseva, and V. M. Shalaev, Science **339** (2013).
[18] N. Yu, P. Genevet, M. A. Kats, F. Aieta, J.-P. Tetienne, F. Capasso, and Z. Gaburro, Science **334**, 333–337 (2011).
[19] A. E. Minovich, A. E. Miroshnichenko, A. Y. Bykov, T. V. Murzina, D. N. Neshev, and Y. S. Kivshar, Laser Photonics Rev. **9**, 195–213 (2015).
[20] F. Aieta, P. Genevet, M. A. Kats, N. Yu, R. Blanchard, Z. Gaburro, and F. Capasso, Nano Lett. **12**, 4932–4936 (2012).

© 2016 The Authors. Laser & Photonics Reviews published by Wiley-VCH Verlag GmbH & Co. KGaA Weinheim.

[21] S. Wang, D. C. Abeysinghe, and Q. Zhan, Opt. Lett. **40**, 4711–4714 (2015).
[22] W. T. Chen, K.-Y. Yang, C.-M. Wang, Y.-W. Huang, G. Sun, I. D. Chiang, C. Y. Liao, W.-L. Hsu, H. T. Lin, S. Sun, L. Zhou, A. Q. Liu, and D. P. Tsai, Nano Lett. **14**, 225–230 (2014).
[23] K. Huang, Z. Dong, S. Mei, L. Zhang, Y. Liu, H. Liu, H. Zhu, J. Teng, B. Luk'yanchuk, J. K. W. Yang, and C.-W. Qiu, Laser Photonics Rev. (2016) 10.1002/lpor.201500314.
[24] L.-J. Black, Y. Wang, C. H. de Groot, A. Arbouet, and O. L. Muskens, ACS Nano **8**, 6390–6399 (2014).
[25] J. B. Khurgin, and G. Sun, Appl. Phys. Lett. **99**, 211106 (2011).
[26] J. B. Khurgin, and G. Sun, Nat. Photonics **8**, 468–473 (2014).
[27] M. Khorasaninejad, F. Aieta, P. Kanhaiya, M. A. Kats, P. Genevet, D. Rousso, and F. Capasso, Nano Lett. **15**, 5358–5362 (2015).
[28] R. Paniagua-Dominguez, Y. F. Yu, A. E. Miroshnichenko, L. A. Krivitsky, Y. H. Fu, V. Valuckas, L. Gonzaga, Y. T. Toh, A. Y. S. Kay, B. Luk'yanchuk, and A. I. Kuznetsov, Nat. Commun. **7** (2016).
[29] Y. Yang, I. I. Kravchenko, D. P. Briggs, and J. Valentine, Nat. Commun. **5** (2014).
[30] P. Moitra, Y. Yang, Z. Anderson, I. I. Kravchenko, D. P. Briggs, and J. Valentine, Nat. Photonics **7**, 791–795 (2013).
[31] N. I. Zheludev, and E. Plum, Nat. Nanotechnol. **11**, 16–22 (2016).
[32] Q. Wang, E. T. F. Rogers, B. Gholipour, C.-M. Wang, G. Yuan, J. Teng, and N. I. Zheludev, Nat. Photonics **10**, 60–65 (2016).
[33] P. Li, X. Yang, T. W. W. Masz, J. Hanss, M. Lewin, A.-K. U. Michel, M. Wuttig, and T. Taubner, Nat. Mater. (2016), doi:10.1038/nmat4649.
[34] S. Raoux, Annu. Rev. Mater. Res. **39**, 25–48 (2009).
[35] H. F. Hamann, M. O'Boyle, Y. C. Martin, M. Rooks, and H. K. Wickramasinghe, Nat. Mater. **5**, 383–387 (2006).
[36] N. Yamada, E. Ohno, K. Nishiuchi, N. Akahira, and M. Takao, J. Appl. Phys. **69**, 2849–2856 (1991).
[37] C. M. Chang, C. H. Chu, M. L. Tseng, H.-P. Chiang, M. Mansuripur, and D. P. Tsai, Opt. Express **19**, 9492–9504 (2011).
[38] R. Pandian, B. J. Kooi, G. Palasantzas, J. T. M. De Hosson, and A. Pauza, Adv. Mater. **19**, 4431–4437 (2007).
[39] T. Motoyasu, M. Takahiro, and O. Takeo, Jpn. J. Appl. Phys. **48**, 080001 (2009).
[40] D. Loke, T. H. Lee, W. J. Wang, L. P. Shi, R. Zhao, Y. C. Yeo, T. C. Chong, and S. R. Elliott, Science **336**, 1566–1569 (2012).
[41] M. Wuttig, and N. Yamada, Nat. Mater. **6**, 824–832 (2007).
[42] F. Xiong, A. D. Liao, D. Estrada, and E. Pop, Science **332**, 568–570 (2011).
[43] B. Gholipour, J. Zhang, K. F. MacDonald, D. W. Hewak, and N. I. Zheludev, Adv. Mater. **25**, 3050–3054 (2013).
[44] Y. G. Chen, T. S. Kao, B. Ng, X. Li, X. G. Luo, B. Luk'yanchuk, S. A. Maier, and M. H. Hong, Opt. Express **21**, 13691–13698 (2013).
[45] A.-K. U. Michel, D. N. Chigrin, T. W. W. Maß, K. Schönauer, M. Salinga, M. Wuttig, and T. Taubner, Nano Lett. **13**, 3470–3475 (2013).
[46] L. Zou, M. Cryan, and M. Klemm, Opt. Express **22**, 24142–24148 (2014).
[47] Y. Noboru, O. Eiji, A. Nobuo, N. Ken'ichi, N. Ken'ichi, and T. Masatoshi, Jpn. J. Appl. Phys. **26**, 61 (1987).
[48] K. Shportko, S. Kremers, M. Woda, D. Lencer, J. Robertson, and M. Wuttig, Nat. Mater. **7**, 653–658 (2008).
[49] J.-W. Park, S. H. Eom, H. Lee, J. L. F. Da Silva, Y.-S. Kang, T.-Y. Lee, and Y. H. Khang, Phys. Rev. B **80**, 115209 (2009).
[50] N. I. Zheludev, and Y. S. Kivshar, Nat. Mater. **11**, 917–924 (2012).
[51] C. F. Bohren, and D. R. Huffman, "Absorption and Scattering by an Arbitrary Particle," in Absorption and Scattering of Light by Small Particles (Wiley-VCH Verlag GmbH, 2007), pp. 57–81.
[52] E. J. Davis, Aerosol Sci. Technol. **12**, 463–464 (1990).
[53] S. Lu Ping, C. Tow Chong, T. Pik Kee, M. Xiang Shui, H. Jia Jun, and W. Yong Jun, Jpn. J. Appl. Phys. **39**, 733 (2000).
[54] M. L. Tseng, B. H. Chen, C. H. Chu, C. M. Chang, W. C. Lin, N.-N. Chu, M. Mansuripur, A. Q. Liu, and D. P. Tsai, Opt. Express **19**, 16975–16984 (2011).
[55] N. V. Voshchinnikov, G. Videen, and T. Henning, Appl. Opt. **46**, 4065–4072 (2007).
[56] G. S. Agarwal, and R. Inguva, Phys. Rev. B **30**, 6108–6117 (1984).
[57] D. E. Aspnes, Am. J. Phys. **50**, 704–709 (1982).
[58] M. Rahmani, D. Y. Lei, V. Giannini, B. Lukiyanchuk, M. Ranjbar, T. Y. F. Liew, M. Hong, and S. A. Maier, Nano Lett. **12**, 2101–2106 (2012).
[59] V. A. Fedotov, M. Rose, S. L. Prosvirnin, N. Papasimakis, and N. I. Zheludev, Phys. Rev. Lett. **99**, 147401 (2007).
[60] Y. Sonnefraud, A. Leen Koh, D. W. McComb, and S. A. Maier, Laser Photonics Rev. **6**, 277–295 (2012).
[61] R. Ameling, and H. Giessen, Laser Photonics Rev. **7**, 141–169 (2013).
[62] Y. Mitsushiro, S. Yasuo, S. Hiroko, K. Takeshi, E. Atsushi, U. Tomokazu, and H. Tohru, Jpn. J. Appl. Phys. **40**, 1578 (2001).
[63] J. B. Lassiter, H. Sobhani, M. W. Knight, W. S. Mielczarek, P. Nordlander, and N. J. Halas, Nano Lett. **12**, 1058–1062 (2012).
[64] S. Sun, K.-Y. Yang, C.-M. Wang, T.-K. Juan, W. T. Chen, C. Y. Liao, Q. He, S. Xiao, W.-T. Kung, G.-Y. Guo, L. Zhou, and D. P. Tsai, Nano Lett. **12**, 6223–6229 (2012).
[65] R. Thielsch, T. Böhme, and H. Böttcher, Phys. Status Solidi A **155**, 157–170 (1996).
[66] J. Wang, S. Qu, H. Ma, Z. Xu, A. Zhang, H. Zhou, H. Chen, and Y. Li, Appl. Phys. Lett. **101**, 201104 (2012).
[67] S. K. Lin, I. C. Lin, and D. P. Tsai, Opt. Express **14**, 4452–4458 (2006).
[68] C. H. Chu, C. D. Shiue, H. W. Cheng, M. L. Tseng, H.-P. Chiang, M. Mansuripur, and D. P. Tsai, Opt. Express **18**, 18383–18393 (2010).
[69] M. L. Tseng, P. C. Wu, S. Sun, C. M. Chang, W. T. Chen, C. H. Chu, P. L. Chen, L. Zhou, D. W. Huang, T. J. Yen, and D. P. Tsai, Laser Photonics Rev. **6**, 702–707 (2012).

© 2016 The Authors. Laser & Photonics Reviews published by Wiley-VCH Verlag GmbH & Co. KGaA Weinheim.